A "Single-Sample Concept" (SSC): A New Approach to the Combinatorial Chemistry of Inorganic Materials

Jürg Hulliger* and Muhammad Aslam Awan[a]

Abstract: Combinatorial estimations show that, within an unreacted ceramic sample prepared by mixing N different starting materials M_xO_y with average particle size ~1 μm, there are about 10^{12} grains per cubic centimeter, sufficient for local reactions to occur that may produce a larger number of product oxides than presently accessible by 2D plate techniques. The "single-sample concept" (SSC) is proposed for performing property-directed syntheses for the preparation of ferri-/ferromagnetic or superconducting compounds. Because of the magnetic properties of the products, libraries of product grains can be sorted by means of magnetic separation techniques. For materials with a large magnetization, the separation efficiency is so high that traces of products can be isolated. The SSC concept was tested experimentally to prepare Fe-based oxides ($N=17$, 24, 30). The large yields (<75 wt%, $N=17$) of product grains agree with the literature data, which indicate that 3d metal magnetic oxide phases ($T_c>300$ K) are most probably Fe oxides. In combination with magnetic separation techniques, SSC seems particularly adapted for exploring the solid-state chemistry of metallic lead elements that form ferri-/ferromagnetic or superconducting oxide phases difficult to detect systematically within the large phase space of theoretically existing compounds.

Keywords: ceramic synthesis · chromatography · combinatorial chemistry · ferromagnetic properties · magnetic separation · superconductors

Introduction

"**…all chemical compounds capable of existence… are already present on the energy landscape and are just waiting to be discovered.**"[1]

Joseph J. Hanak's idea of the "multiple sample concept" (MSC)[2] has, within the last 10 years, found widespread application through 2D plate approaches, in which pixel-sized elemental compositions for *parallel syntheses* have been prepared by mixing starting materials through the vapor or liquid phase. Many analytical techniques have been developed to perform phase and property analyses in parallel.[3–8] As the number of initial elemental starting compositions on one reaction plate has reached more than 25000, combinatorial synthesis may be considered "the first rational concept to tap the potential wealth of chemical diversity in a more systematic way."[5] Combinatorial chemistry now makes the exploration of the diversity of certain compound classes a realistic endeavor.

[a] Prof. Dr. J. Hulliger, M. Aslam Awan
Department of Chemistry and Biochemistry
University Berne, Freiestrasse 3, 3012 Berne (Switzerland)
Fax: (+41) 31-631-3993
E-mail: juerg.hulliger@iac.unibe.ch

However, realistic restrictions are required to limit both the number of starting components (N) and the number of elements (q) per compound formed, otherwise the combinatorial functions will far exceed the feasibility of any practical synthesis. Given these general constraints, we may, nevertheless, attempt to find a solution to the impossible[9] by asking: What is the minimum number of, for example, metallic elements in a crystal structure or amorphous phase that can provide sufficient chemical diversity to be able to determine the conductive, magnetic, luminescent, or catalytic properties of the material?

High-temperature superconductivity[10] is possible for $q=$ 3–4 metallic elements. Other important properties, such as ferri-/ferromagnetism, luminescence and catalysis, have been determined for only $q=2$–3. In recognition of the many possible properties of a material, we can assume that novel properties or advanced performance of known compounds might be obtained with a small number of constitutional metals in oxides, halogenides, sulfides, and so forth.

Therefore, present estimations concerning the "existing"[1] phases to be prepared by new combinatorial syntheses with N components as starting materials are limited to $q\leq 6$ (the number of constitutional metals in, for example, oxide compounds). Given N building blocks, these components are grouped to constitute binary ($q=2$), ternary ($q=3$), etc. (T,x) phase diagrams ($P(O_2)$ defined by the experimental

  DOI: 10.1002/chem.200400231

conditions), for which we can attribute an average number η_q ($q=2$–6) of solid phases present in each diagram. The average maximum number of N_{oxides} phases to be synthesized is thus given by Equation (1):

$$N_{\text{oxides}} \cong \sum_{q=2} \eta_q N_q^{\text{PD}} \quad (1)$$

in which N_q^{PD} is the number of unknown phase diagrams, calculated from Equation (2) (N is the number of building blocks; $q=2$ (binary), $q=3$ (ternary), etc.).

$$N_q^{\text{PD}} = \frac{N!}{q!(N-q)!} \quad (2)$$

What is a realistic estimate for η_q? Although the available phase diagrams for oxides[11] are by no means complete, they are considered representative to gain an estimate of the diversity of solid phases (η).

In the case of $q=2$, the average number of binary metallic oxides is about three (100 representative diagrams selected from volumes I–VIII of reference [11]), whereas the percentage of purely eutectic binary diagrams is ~10% (for a sample of 470 diagrams[11]). For ternary systems, a rough estimate of η_3 yielded only two (86 suitable diagrams;[11] here, because of incomplete compositional scans, η may be higher). This allows us to conclude that the upper limit of η_6 is certainly lower than, say, 100 (number of $E_iE_jE_kE_lE_mE_nO_y$ phases of a certain stoichiometry).

This means that the number of oxide phases a combinatorial procedure will have to provide access to is less than $N_{\text{oxides}} \approx 100 N_6^{\text{PD}}$. The number of phase diagrams for increasing N is shown in Figure 1: by varying N (10–61; the maximum number of nonradioactive metallic elements), we can conclude that a realistic upper limit for N_{oxides} is about 6×10^9 ($N=61$, $q=6$, $\eta_{\max}\approx 100$). Consequently, the corresponding number of experiments are required to explore this diversity. The present combinatorial techniques are still far from this upper limit; however, they have led to the discovery of new phases by varying N from about 10 to 30.

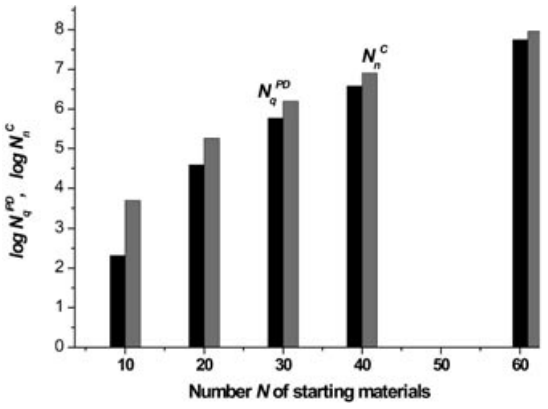

Figure 1. Calculated number of possible phase diagrams N_q^{PD} and local configurations N_n^{C} for N starting components and $n=6$ elements in product grains.

We present here a new method for performing combinatorial syntheses using the "single-sample concept" (SSC): mixing together N micrometer-sized starting oxides to prepare a ceramic sample (see Figure 2), yielding randomly packed particles representing different components and sizes. A combinatorial variety of local compositions (called configurations, N_n^{C}) is generated which establishes 1) elemental and 2) stoichiometric variation. The elemental variation constitutes phase diagrams of order q, along with stoichiometric variation (n), whereas the particle size distribution populates the compositional axes of the phase diagrams.

Figure 2. Mechanical model of spheres of different colors and sizes to visualize *local configurations*, that is, grain contacts by n starting grains, to obtain the diversity of product grains distributed within the bulk sample.

A combinatorial estimation of the number N_n^{C} shows that it can be larger than the number N_q^{PD} of phase diagrams [see Figure 1 and Eq. (3)]:

$$N_n^{\text{C}} < \binom{N+n-1}{n} \quad (3)$$

(excluding those configurations consisting of the same elements; n is the number of grains in a configuration, $n \geq q$).

The SSC therefore provides access to the manifold of phase diagrams. As N_n^{C} is of the same order as N_q^{PD} (see Figure 1; $n \approx q$), the particle size distribution is required to provide a dense population of the compositional axes of the phase diagrams. Finally, we have to make sure that a typical sample of about 1 cm^3 contains sufficient grains for both the elemental and size distribution: in the case of an average grain size of 1 μm, there are about 10^{12} grains per cubic centimeter. Assuming a reasonable number of components (10–40), the number of grains is orders of magnitude larger than the estimated number of oxide phases. The number, $N_{\text{p,}}$ of micrometer-sized product grains per phase is of the order of 10^6 to 10^3 ($N=10$–40), which, if given in ppm, is a small density, generally below a few ppm ($N>10$).

The SSC thus provides access to a library that may unravel a defined (N, q, η) chemical diversity for a selected class

of compounds. Once such a library is obtained, we face the task of how to read it.

Today's analytical techniques have reached a resolution down to the nanometer size, both for compositional and structural analysis.[12] Nevertheless, property characterization is much more difficult using the present concept than when applying 2D plate techniques. However, if we focus on specific properties, such as, those of ferri-/ferromagnetic or superconducting materials, highly efficient particle separation techniques can be applied. Consequently, we have introduced *magnetic separation* into materials chemistry that allows particle extraction for micrometer-sized product phases.

SSC may be applied in different ways:

1) A mixture of similar amounts (mass, volume, or moles) of N metal oxides reacts to form q-type oxides. In this case, oxygen is the lead (L) element without a preference for any one metal in setting up the starting composition.
2) A "lead oxide" is added in a larger quantity than the other constituents in order to preferentially form $E_iE_jE_L\ldots O_y$ instead of $E_iE_jE_k\ldots O_y$ ($i,j,k,\ \ldots,\neq L$) compounds.

In the present study we concentrate on the second application by using Fe to produce a diversity of iron oxides with a selected number N (17, 24, 30) of nonmagnetic elements. Lead element Fe was selected to demonstrate the feasibility of SSC in combination with magnetic separation. In further studies SSC will be applied to search for i) new ferri-/ferromagnetic 3d transition metal oxides and ii) superconductors.

Results and Discussion

Isolation of product phases by magnetic separation: A single-sample combinatorial synthesis may produce a small number (N_p) of product grains representing the material of interest. In most cases, bulk analysis would not be successful, thus making separation techniques necessary. In the case of either strongly ferri-/ferromagnetic or superconducting materials, magnetic separation can be applied.

Magnetic separation of mixtures of small particles exhibiting different magnetic properties is achieved by the action of an inhomogeneous magnetic field, which leads to the attraction (ferri-, ferro-, para-, or superparamagnetic) or deflection (diamagnetic) of particles dispersed in a gas or fluid passing through the separator column.[13,14] As samples show different particle size and magnetization strength distributions, "magnetic chromatography"[15–17] offers a new technique for separating particles according to their size and magnetization. In industry, large-scale magnetic separation using conventional or superconducting magnets, so-called high gradient magnetic separation (HGMS),[18] is applied in the purification of minerals (kaolin, talc) and is used in mining to recover ores (hematite, siderite, elite).[19]

In material science, magnetic separation was mainly applied to separate, purify, and characterize ceramic copper oxide superconductors. Simple equipment allowed the deflection of grains of superconducting phases at liquid nitrogen temperature.[20–27] However, solid-state chemistry has not yet made systematic use of this technique to extract phases from, for example, a combinatorial synthesis.

The magnetic force $\boldsymbol{F}$ exerted on a particle is given by Equation (4):[28]

$$\boldsymbol{F}_z = \frac{\chi}{\mu_0} V \boldsymbol{B} \frac{\partial \boldsymbol{B}_z}{\partial z} \tag{4}$$

in which $\boldsymbol{B}$ is the magnetic induction, z the direction of the gradient, V the particle volume, χ the magnetic susceptibility (here assumed to be isotropic), and μ_0 the permeability of the vacuum.

The magnitude of the force is thus proportional to the product of the field strength and its gradient. The mechanical action is along the field gradient. In a practical setup, generation of the strongest field inhomogeneity is given by ferromagnetic wires (wool or a sieve). The maximum force has been estimated for a wire diameter of two to three times the particle size.[20,29] Given today's ultra-high-field magnets (pulsed), there are many prospective applications for magnetic particle separation in materials science. In the case of superconductors, however, $\boldsymbol{B}$ must be less than $\boldsymbol{B}_c$, the critical field above which diamagnetism decreases. Here, the gradient has to be maximized. Furthermore, superconductive particles must be sufficiently large because of the London penetration depth.[30]

An important issue in particle separation is aggregation, that is, cake formation.[31] In our case there are three origins of aggregation:

1) Synthesis can yield multiphase particles (e.g., intergrown ferri-/ferromagnetic and diamagnetic phases) that are not separated by ball-milling.
2) Single or multiphase particles suspended in a fluid can aggregate owing to of interactions between surfaces. Practical separation in industry therefore uses surfactants.
3) Aggregation can occur due to ferri- or ferromagnetic interaction.

Our laboratory setup for the continuous extraction of, for example, ferri-, ferro–, para-, or superparamagnetic (T= 300 K) particles from a suspension is shown in Figure 3: particles pass through a column surrounded by permanent magnets and stick to the walls of the column (Figure 3a), or a vertical tube is filled with magnetic sieves (mesh size ~ 75 μm) surrounded by a number of permanent magnets (Figure 3b). A low-density suspension (activated by ultrasound) is continuously pumped through the column. After the first separation step, only fluid is passed through the column to wash out retained nonmagnetic particles. The magnets are then removed to release the magnetic particles from the walls (Figure 3a) or sieves (Figure 3b). $B_8Fe_{77}Nd_{15}$ magnets were used in all systems.

In the case in which the column is filled with horizontal sieves (Figure 3b), we may define the probability $P_{i,i+1}$, to

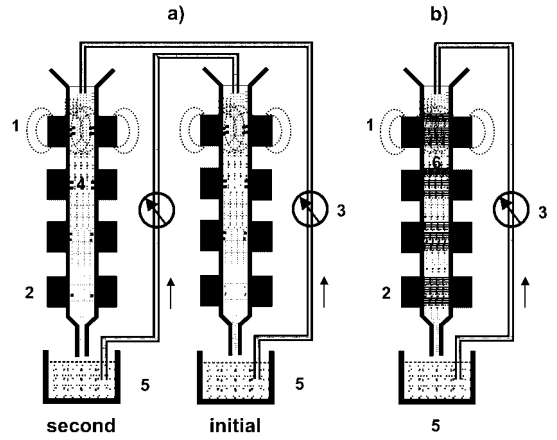

Figure 3. Two types of magnetic separators used to extract magnetic particles from a SSC reaction mixture: a) vertical column exposed to a magnetic field (1) from permanent magnets (2). A liquid carrying product grains is pumped (3) through the column. Magnetic particles stick (4) at locations of strong magnetic gradients. For disaggregation of particles the liquid is continuously passed through an ultrasonic bath (5). b) Similar to a), using 75 μm wide horizontal magnetic sieves (6) to retain magnetic particles by the strongly inhomogeneous field on the sieves.

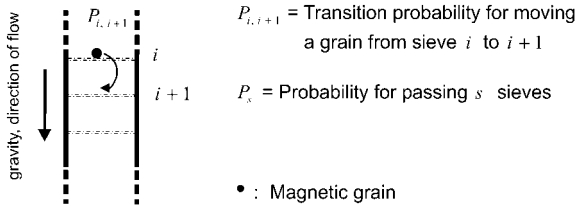

Figure 4. Estimation of the probability for passing grains through a magnetic column (see also Table 1).

describe the translocation of a grain from sieve i to sieve i+1 (Figure 4). As a grain has to pass through all s sieves in order to exit the column, the probability of passing through the entire column is given by Equation (5).

$$P_s = (P_{i,i+1})^s \quad (5)$$

Table 1 gives realistic data for P_s that cover low to high $P_{i,i+1}$ values. For the present separators (Figure 3b), s is approximately ten. New separators providing $s = 1000$–3000 are under development. Strongly ferromagnetic particles can overcome the effect of gravity and forces imposed by the flow of the liquid. For strong forces, $P_{i,i+1}$ for these materials is almost zero. Consequently, the retention efficiency for strongly magnetic materials is nearly 100%. Although superconducting materials show different behavior in an inhomogeneous magnetic field, it is nevertheless unlikely for grains to pass efficiently through a column of large s. Therefore, the separators shown in Figure 3b show great potential for the extraction of small fractions of superconducting materials in SSC syntheses.

Table 1. Probability P_s of particles passing through a series of s sieves.

$P_{i,i+1}$	P_s		
	$s=10$	$s=100$	$s=1000$
0.01	0	0	0
0.10	1.0×10^{-10}	0	0
0.50	9.8×10^{-4}	0	0
0.90	0.35	2.7×10^{-5}	0
0.99	0.90	0.37	4.3×10^{-5}
0.999	0.99	0.90	0.37

The separation efficiency was tested experimentally by passing a mixture of Al_2O_3, La_2O_3, TiO_2, ZnO and ZrO_2, and $BaFe_{12}O_{19}$ (10 and 20 wt%) particles in water, containing a surfactant[32] (Decon 90 and NH_4OH(aq.)), through the column (see Figure 3a). The separation ($BaFe_{12}O_{19}$) yield was 10 and 20 wt%, respectively. For trace analysis, about 1 ppm (wt) of $BaFe_{12}O_{19}$ grains in a mixture with nonmagnetic oxide powder was passed through the column. Using magnetic sieves, some ferromagnetic particles were recovered, showing that, in principle, a pin could be found in a haystack!

Results for magnetic oxides: The preparation of configurations [Eq. (3)] requires a dense population of grains that undergo local reactions. Mixing N starting oxides M_xO_y by ball-milling (adding a liquid to improve homogenization) and pressing into a pellet is known as the classical ceramic preparation. Long-term ball-milling may achieve elemental homogenization and reduce the particle size. Scanning electron microscopy and mapping of the elements confirmed this. Major difficulties in bringing such a sample to reaction may involve 1) liquid formation (eutectic compositions and low-melting compounds) and 2) spreading of elements over the sample because of high vapor-pressure components.

In experiments with $N = 10$–30, M_xO_y, reaction temperatures in the range 1000–1100 K, and reaction times of minutes to hours: 1) visual inspection of pellets, 2) DSC, and 3) SEM showed no evidence for significant liquid-phase formation. Transmission electron microscopy (qualitative elemental analysis) performed on 30 single particles in the range 100–300 nm confirmed crystalline particles reflecting a broad distribution of elemental compositions. The average number of different elements in the grains was six to seven (for 12 M_xO_y starting materials used for the basic test). The starting materials (except for the lead element) were mostly consumed. Powder X-ray diffraction showed no evident background scattering; this would be typical of amorphous phases. In view of the many compound N_{oxides} a sample might contain, the number of intense diffraction lines was generally very small. For most phases the net amount per phase was probably too low or the number of grains per phase was not sufficient to produce a sharp powder pattern.

Configurations in bulk ceramic samples interfere with and share grains for reaction. Compared with powder samples, the reaction of isolated aggregates of particles would match the conditions set up by Equation (3) more reasonably. A surface providing support for configurations N_n^C would thus be of great use. Currently, we are working with sodium chloride to disperse aggregated M_xO_y starting grains onto NaCl particles ($\langle d\rangle_{\text{NaCl}} \gg \langle d\rangle_{\text{oxides}}$). By keeping the reaction temperature below melting, the NaCl surface in the state of (eutectic systems) liquid formation may enhance reactivity and promote crystallization of single-phase grains. The reaction of NaCl with most oxides should not present a serious prob-

lem (i.e., solid solution and oxy–chloride formation), as NaCl is commonly used in the flux growth of various oxide compounds. After the reaction, dissolution of the supporting material preferentially liberated particles, showing a smaller degree of intergrowth than those obtained from the powder sample. Both routes were explored to synthesize ferri-/ferromagnetic materials.

Selecting Fe as the "lead" element, databases provided the rather small number of about 53 ferri- or ferromagnetic Fe oxides ($T_c > 300$ K, containing no other magnetically active element). In the case of V, Cr, Mn, Co, and Ni, the number of compounds characterized is even smaller

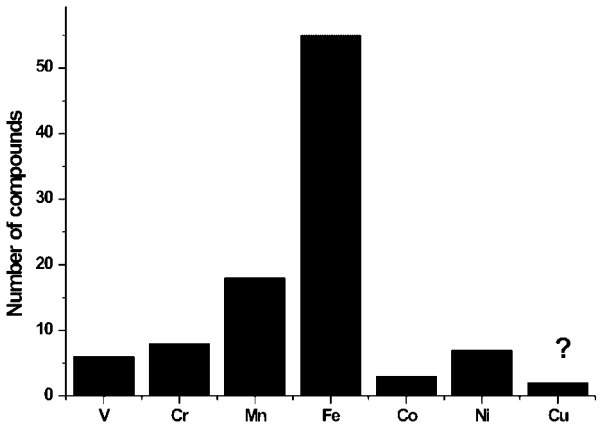

Figure 5. Results of a literature search for ferri- and ferromagnetic M(3d) oxides ($T_c > 300$ K). The search clearly found more Fe oxides than other 3d metals.

(Figure 5). For Cu, only one class of compounds ($MgCu_2O_3$, Ca_2CuO_3, $BaCuO_3$)[33,34] was found for which evidence of ferromagnetic coupling above 300 K is reported. However, these structures, as expected, show 1D antiferromagnetic ordering. Excess oxygen is reported to induce spin flips and ferromagnetic interchain coupling.[35] Given present knowledge, Fe seems to be the leading 3d transition element for obtaining magnetic oxides ($T_c > 300$ K).

For SSC syntheses, we started from 17 (Li, Na, Mg, Si, K, Ca, Sr, Y, Nb Mo, Sn, Te, Ba, La, W, Pb, Bi), 24 (Li, B, Na, Mg, Al, Si, K, Ca, Ti, Ga, Ge, Sr, Y, Zr, Nb, Mo, In, Sn, Te, Ba, La, W, Pb, Bi) or 30 (Li, B, Na, Mg, Al, Si, K, Ca, Ti, Zn, Ga, Ge, Rb, Sr, Y, Zr, Nb, Mo, Cd, In, Sn, Te, Cs, Ba, La, Ta, Hf, W, Pb, Bi) elements ($M \neq Fe$; equal amounts in wt% of each oxide) to which was added a variable amount of Fe_2O_3, ranging from 5 to 25 wt%. Metals were added in the form of oxides, peroxides, and carbonates. For mixing and downsizing, starting materials were ball-milled (achat mortar and balls; added isooctane for improvement of mixing) for 2–3 h. The average particle size after ball-milling was in the same range as found after sintering, as determined by scanning electron microscopy (SEM).

We distinguish two different routes.

Route I—ceramic bulk sample preparation: The mixture of components was pressed into several pellets, yielding a total volume of 1 cm^3. The pellets were filled in a ceramic (Al_2O_3) boat that was placed in a horizontal furnace (quartz tube), heated at a rate of 150 $K\,h^{-1}$, held at 1126 K for 2 h and then the temperature was reduced at a rate of 100 $K\,h^{-1}$. An oxygen flow of ~600–800 $mL\,h^{-1}$ was passed through the furnace at 1 atm.

After heating, pellets, on average, showed a weight loss Δg of ~10–15%, a reduction in diameter of 10–15%, and a ruduction in thickness of ~5–10%, and were not deformed. The color appeared to be homogeneous (yellowish brown). SEM pictures (Figure 6) showed a homogeneous polycrystalline sample with a particle size of ~100–900 nm. Prior to magnetic separation, the reacted samples were ball-milled (1.5 h, in isooctane), dried, and dispersed (ultrasound) in water containing a surfactant (Decon 90 plus $NH_4OH_{(aq)}$). This may result in the loss of some compounds by reaction with water. However, dispersing the samples in water did not give rise to a significant change in pH. For separation, the suspension was first pumped (Figure 3) through an ultrasonic bath before entering the separator column (Figure 3a).

Surprisingly high yields of magnetically retained grains were obtained (Figure 7): on varying the content of Fe_2O_3 from 5 to 25 wt%, corresponding yields of 7.5 to 75 wt% were obtained. Passing the separated particles through the column a second time did not improve the yield significantly. Although ball-milling disaggregates intergrown particles, it is likely that diamagnetic material adheres to the ferri- or ferromagnetic crystallites to some extent. The effective yields are thus certainly smaller than shown in Figure 7.

In view of the many compounds which could possibly form (see Figure 1), the powder X-ray diagrams did not show as many lines as expected (see Figure 8): the rather weak scattering intensity of a few of the lines may be indicative of compounds that were preferably formed under the

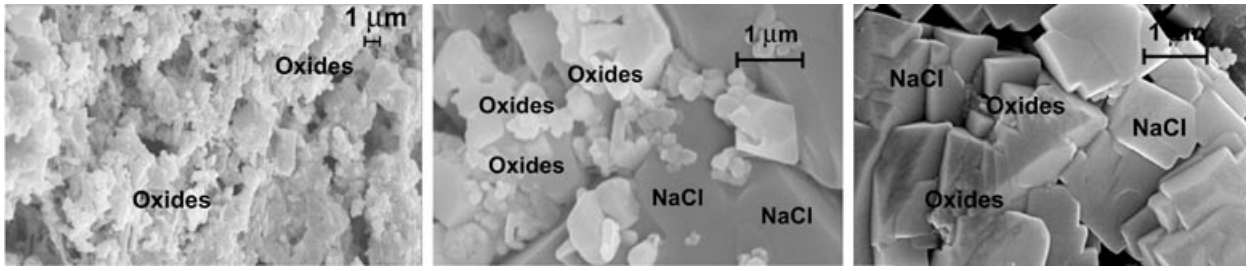

Figure 6. SEM micrographs showing the particle morphology for the SSC (inside the pellets): Left) 17 oxides including 15 wt% Fe_2O_3, route I (see text). Middle) 17 oxides including 15 wt% Fe_2O_3, route II (see text). Right) Same as that in the middle, but prior to reaction: unreacted oxides particle are distributed over the surface of the NaCl crystals.

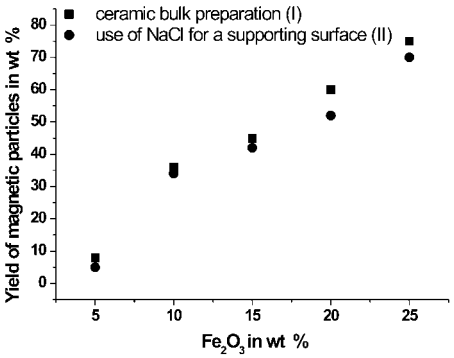

Figure 7. Yield of magnetic particles retained by the magnetic separation column shown in Figure 3a. Example of 17 oxides and a variable amount of Fe_2O_3. Results for the products from routes I and II (see text) show very similar yields, although the particle morphologies are clearly different (see Figure 6).

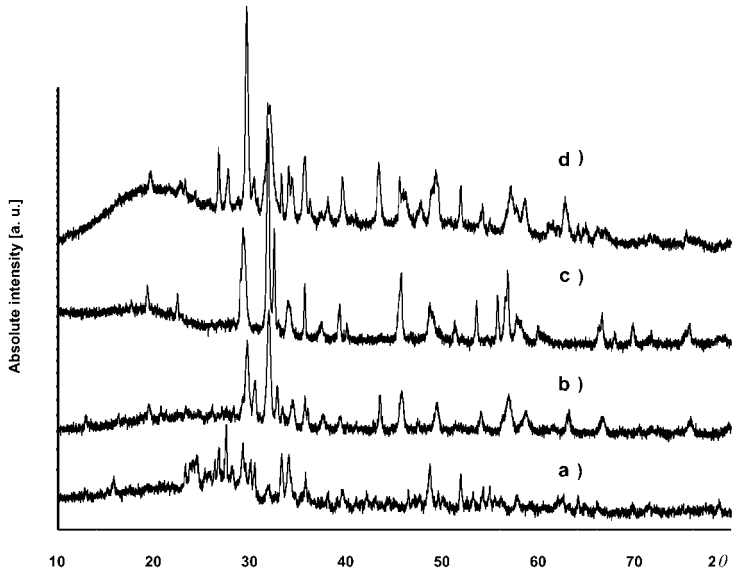

Figure 8. X-ray diffraction patterns of SCC samples (17 elements plus 15 wt% Fe_2O_3): a) prior to reaction, b) after reaction, c) after magnetic separation, and d) reaction performed on NaCl(s).

present conditions. Using all the data available in the X-ray powder diffraction PDF file, no significant matching with any known compound containing elements we used was possible. Powder diffraction is probably not very helpful in this case for analyzing SSC products, as evident from comparing the X-ray diagrams of magnetically separated samples with that of as-obtained and residual powder: in all three cases, the most intense lines present in Figure 8 were present. Changes were only observed for weak lines. However, the powder diffraction diagrams revealed an important fact: the starting materials were consumed.

Route II—use of NaCl as a supporting surface: In this case we proceeded in the same way, except that an additional ball-milling step (2–3 h, in isooctane) was applied to load the NaCl particles with premixed (ball-milled) oxide particles (10 wt% oxides, 90 wt% NaCl; see Figure 6, right). The reaction was performed at a maximum temperature of 1026 K. After heating, the pellets appeared homogeneously colored (dark brown) and showed no significant deformation. We take this as an indication that, also in this case, liquid-phase formation was not a dominant process. Figure 6 shows the inner surfaces of typical pellets. Although the reaction temperature was 100 K lower than for route I, the yield of magnetic particles in the case of Fe was nearly the same for both routes. From this we can conclude that local reaction mixtures form various kinds of solid materials. It is likely that, on the surface of the NaCl particles, a liquid film which dissolves the oxides is involved in the reaction and the crystallization of new phases. Figure 6 shows small crystallites (~100–900 nm) on top of much larger NaCl particles, most of which show crystal faces. The degree of intergrowth can be seen to be much less than for route I (Figure 6 left). The powder X-ray diagrams of the materials obtained from route II are very similar to those obtained by route I, although a difference with respect to the weak lines can be seen in Figure 8.

Although higher reaction temperatures can be used when employing a nonreactive support, there are not many salts available for this purpose. $BaCl_2$ (melting point 1236 K) may provide an extension of about 100 K over NaCl. Improvements to route II would include a reduction in the degree of loading of NaCl particles by oxides in order to obtain a lower degree of aggregation of product particles, preferably many single particles. A low degree of aggregation will be needed to be able to use single-particle analyses (compositional and structural).

Confirmation of the presence of ferri- or ferromagnetic materials was obtained from susceptibility measurements (7.5, 10, 15, and 20 wt% Fe_2O_3; 17 M_xO_y, route I, and 15 wt% Fe_2O_3, route II): hysteresis loops were recorded (Figure 9). Table 2 summarizes the data obtained for the SSC for different amounts of Fe_2O_3.

Because superparamagnetic behavior is expected for iron oxides with a particle size smaller than about 10 nm,[36] we assume that the present particles (on average 10–90 times larger) are in the ferro- or ferrimagnetic state. When we have many hysteresis loops characterizing the individual compounds of a mixture, there are upper and lower limits for M_s (saturation magnetization), M_{rem} (remanent magnetization) and H_c (coercive field). The superposition of all data can result in a rather narrow hysteresis curve, as shown in Figure 10. For a mathematical demonstration we have taken a tangent hyperbolic to approximate a hysteresis loop: $M \approx \alpha \tanh(\beta H + \gamma)$, where values for α, β, and γ were selected

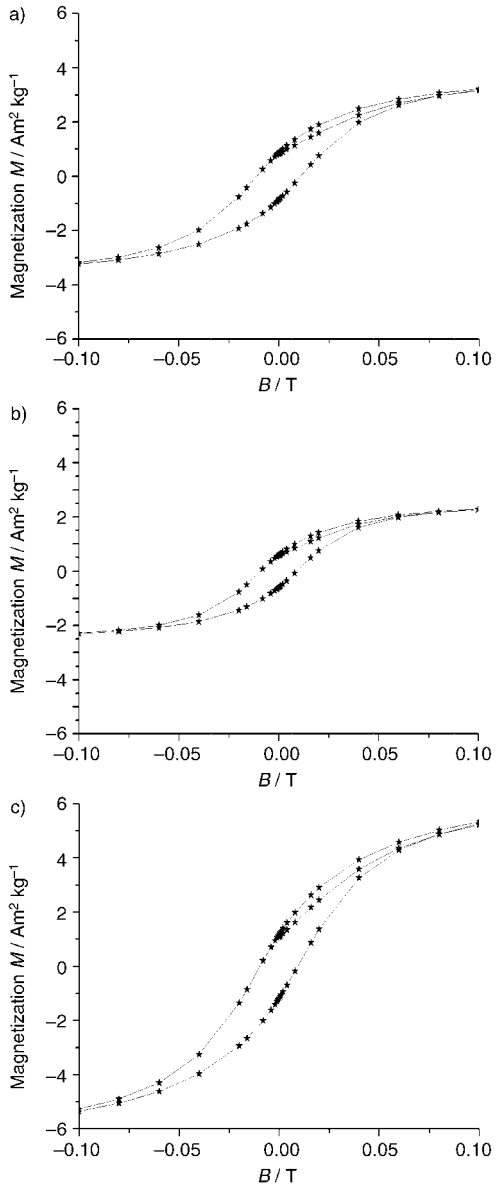

Figure 9. Hysteresis loops for typical SSC products. All measurements started at $\boldsymbol{B}=0$ T ($T=300$ K). Loops were recorded after magnetic separation by the separator shown in Figure 3a. a) 10 wt% Fe_2O_3 plus 17 elements, ceramic route I; b) 15 wt% Fe_2O_3 plus 17 elements, ceramic route I; c) 15 wt% Fe_2O_3 plus 17 elements on NaCl, route II.

randomly from fixed intervals to generate a large number of curves which were summated.

The present samples have a saturation magnetization which is about 5–10% of that of a strongly magnetic reference material ($BaFe_{12}O_{19}$). This may be interpreted in two ways: 1) SSC syntheses produced mostly weak ferri- or ferromagnetic materials, or 2) there were large individual M_s components, but adherent nonmagnetic particles reduced the M_s value. Interestingly, samples of 15 wt% Fe_2O_3 (routes I and II) produce almost the same particle yield (see Figure 7), but the synthesis with NaCl produces a material with a much higher M_s.

To gain insight into the elemental distribution of the particles, we performed qualitative elemental analyses using

Table 2. SQUID measurements for SSC products.

Fe_2O_3 [wt%][a]	m [emu][b]/ sample weight [mg]	M_s (300 K, $\boldsymbol{B}=5$ T) [A m^2 kg^{-1}][c]
10(I)	0.44/11.1	4.0
15(I)	0.040/14.9	2.7
15(II)	0.092/13.5	6.8
20(I)	0.060/13.7	4.4
25(I)	0.027/15.1	1.8
$BaFe_{12}O_{19}$[38]	0.330/6.12	54[d]

[a] Reaction conditions: 17 nonmagnetic elements and various wt% of Fe_2O_3; Routes I and II: see text for method of sample preparation. [b] Measured on a Quantum Design SQUID magnetometer (XL5S) at 300 K. m = magnetic moment. [c] M_s = saturation magnetization; for simple Fe oxides: $M_s \leq 100$ (300 K).[36] [d] 76 gauss cm^2 g^{-1}, $\boldsymbol{B}=0.6$ T, extrapolated to zero kelvin.[39]

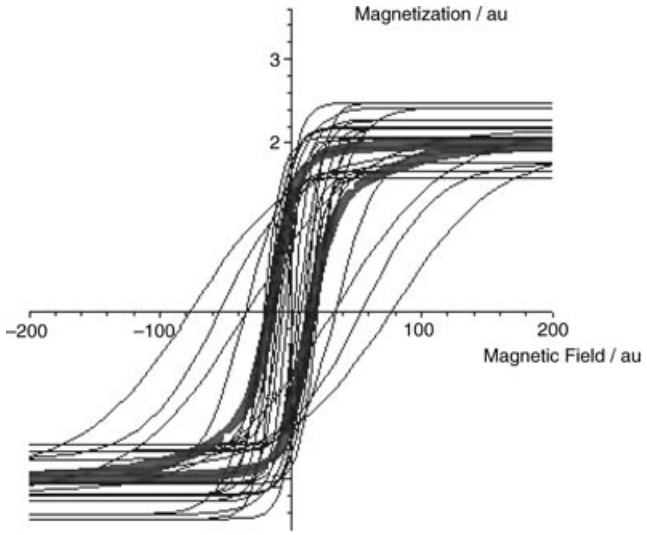

Figure 10. Numerical example showing how a large number of individual hysteresis loops can be summed to form an observable curve (see Figure 9) for samples containing many different particles in the magnetic state. The average field $<H_c>$ may be much smaller than the individual H_c fields. Number of summed curves: 15 (tanh function assumed).

scanning electron microscopy (see Table 3). As some elemental emission lines overlap, we extracted those of the most probable elements present. Clearly, these randomly se-

Table 3. Results of qualitative analysis of the particles using scanning electron microscopy.[a]

Grains	Main elements detected[b]	Compounds from literature[c]
1	Fe > Mg, Ca > Sr, Si > Pb	$MgFe_2O_4$, $CaFe_{15}O_{25}$, $MoFe_2O_4$
2	Fe > Ca, Mg, Sn > Sr, Ba, Bi	$SrFe_{12}O_{19}$, Ca_2MoFeO_6, $Li_{0.5}Fe_{2.5}O_4$
3	Fe > Ca, Mg > Sn, Pb	$Y_3Fe_5O_{12}$, $PbFe_{12}O_{19}$, Sr_2MoFeO_6
4	Fe, Mg, Ca > Sr, Nb	$Ba_{1.6}Sr_{0.4}MoFeO_6$
5	Fe, Ca > Pb	$Ba_{1.28}Sr_{0.32}La_{0.4}MoFeO_6$, $Nb_{0.5}PbFe_{0.5}O_3$
6	Ca > Fe > Sr, Mg	
7	Fe, Ca, Mg > Y, W	
8	Ca > Fe, Mg > La, Mo, Si	

[a] Elements used for SSC: Fe, Li, Na, Mg, Si, K, Ca Sr, Y, Nb, Mo, Sn, Te, Ba, La, W, Pb and Bi. [b] Elements are listed in order of abundance; an energy dispersive spectrometer (Noran IXNSS200) was used. [c] Main compounds found in the literature with $T_c > 300$ K ($q \geq 2$) containing elements used in this study.

lected grains mostly reflect Fe oxides formed by Ca, Mg, and Sr, as well as Sn, Pb, and other elements. Known compounds ($T_c > 300$ K, Table 3) contain mostly Ca, Mg, Sr, Ba, Mo, Pb, and Y, and also Sn, La, and Nb. Of the 17 elements we used, only K, Te, and Li (not detectable) were not found. From the small number of grains we examined we at least can conclude that the SSC produced typical Fe oxides.

Conclusions

As " all chemical compounds capable of existence (with a certain lifetime) are already present on the energy landscape, and are just waiting to be discovered "[1], all we have to do is to establish effective and property-directed procedures for preparing and isolating compounds of interest. In view of the very large phase space (composition, *T*, *P*, and also time) given by a combinatorial function determining the number of phase diagrams (N_q^{PD}), and an unknown number (η_q; which may be accessible using theoretical methods[37]) of thermodynamically stable/metastable compounds appearing in the phase diagrams, it is logical that only a combinatorial approach based on combinatorial functions of the same power will provide access to the existing chemical diversity. We have demonstrated that the number N_n^C of local configurations can be larger than the number N_q^{PD} of local phase diagrams, and that the number of grains (including their size distribution) can even exceed the number $\eta_q \approx$ 100 times N_q^{PD}.

A second innovation with respect to materials chemistry concerns the application of magnetic separation columns, which can attain an extremely high separation efficiency for strongly magnetic materials. The combination of SSC synthesis and magnetic separation is thus considered a new approach for detecting *traces* of magnetic and probably also superconducting materials.

So far we have focussed on thermodynamically stable compounds. The present concept, however, is also suited to obtaining transient products merely by the application of short-term reaction techniques from the field of ceramic materials. Summarizing the experimental results, we have shown that we can obtain high yields of magnetic particles in the case of Fe-based oxides. This is reflected by a comparison of our results with those in the literature.

With the aim of determining the chemical composition of the SSC products, we are working on lead elements E_L that may provide a very low yield of product grains. This brings the analysis of individual grains within practical feasibility. There are two evident goals of interest: $T_c > 300$ K for i) ferri- or ferromagnetic oxides involving Cu, and ii) oxide superconductors.

Acknowledgements

J.H. would like to thank the MPI for Solid-state Research, Stuttgart (group of Professor A. Simon), for the opportunity of a sabbatical in 2000, where the SSC work was started and first presented (18 July 2000). We thank Dr. L. Kienle and B. Frey for the microscopy analysis, Professor S. Decourtins for the use of susceptibility equipment, Dr. W. Marx and T. Samtleben for the literature search, C. Belandinelli for calculating the hysteresis loop, and B. Trusch for technical assistance.

[1] M. Jansen, *Angew. Chem.* **2002**, *114*, 3896–3917; *Angew. Chem. Int. Ed.* **2002**, *41*, 3746–3766.
[2] J. J. Hanak, *J. Mater. Sci.* **1970**, *5*, 964–971.
[3] B. Jandeleit, D. J. Schaefer, T. S. Powers, H. W. Turner, W. H. Weinberg, *Angew. Chem.* **1999**, *111*, 2648–2689; *Angew. Chem. Int. Ed.* **1999**, *38*, 2494–2532.
[4] W. F. Maier, G. Kirsten, M. Orschel, P.-A. Weiss, A. Holzwarth, J. Klein, *ACS Symp. Ser.* **2002**, *814*, 1–21.
[5] E. Dainelson, X. D. Wu, *Science* **1998**, *279*, 837–839.
[6] E. J. Amis, X-D. Xiang, J-C. Zhao, *MRS. Bull.* **2002**, *27*, 295–297 (issue on combinatorial material science).
[7] S. H. DeWitt in *Combinatorial Chemistry: Synthesis and Application* (Eds.: S. R. Wilson, W. Czarnik), Wiley-Interscience, New York, **1997**, pp. 25–38.
[8] C. L. Chen, P. S. Strop, M. Lebl, K. S. Lam in *Combinatorial Chemistry*, 2nd ed. (Eds.: J. N. Abelson, M. I. Simon), Academic Press, New York, **2003**, pp. 211–219.
[9] F. J. DiSalvo, *Pure Appl. Chem.* **2000**, *72*, 1799–1807.
[10] C. P. Poole, Jr, A. P. Ramirez, P. C. Canfield in *Superconductivity* (Ed.: C. P. Poole, Jr.), Academic Press, New York, **2000**, pp. 71–108.
[11] a) B. O. Mysen in *Phase Diagrams for Ceramists, VIII*, ACS, Ohio, **1990**; b) L. P. Cook, H. F. McMurdie, H. M. OndikK. M. Kessell, M. J. Rodtely in *Phase Diagrams for Ceramists, VII*, ACS, Ohio, **1989**; c) R. S. Roth, J. R. Diennis, H. F. Mc Murdie in *Phase Diagrams for Ceramists, VI*, ACS, Ohio, **1987**; d) R. T. Negas, L. P. Cook in *Phase Diagrams for Ceramist, Vs*, ACS, Ohio, **1983**; e) L. P. Cook, R. Lowrance in *Phase Diagrams for Ceramists, IV*, ACS, Ohio, **1981**; f) E. M. Levin, H. F. Mc Murdie in *Phase Diagrams for Ceramists, III*, ACS, Ohio, **1975**; g) E. M. Levin, C. R. Robbins, H. F. Mc Murdie in *Phase Diagrams for Ceramists, II*, ACS, Ohio, **1969**; h) E. M. Levin, C. R. Robbins, H. F. Mc Murdie in *Phase Diagrams for Ceramists*, ACS, Ohio, **1964**, *II*.
[12] A. Carlsson, T. Oku, J.-O. Bovin, R. Wallenberg, J.-O. Malm, G. Schmid, T. Kubicki, *Angew. Chem.* **1998**, *110*, 1275–1278; *Angew. Chem. Int. Ed.* **1998**, *37*, 1217–1220.
[13] "The Physical Principles of Magnetic Separation"J. Svoboda in *Magnetic Methods for the Treatment of Minerals*, Elsevier, Amsterdam, **1987**, pp. 1–76.
[14] J. Boehm, *IEEE. Trans. Appl. Supercond.* **2000**, *10*, 710–715.
[15] T. Ohara, S. Mori, Y. Oda, Y. Wada, O. Tsukamoto, *Trans. IEE Jpn.* **1996**, *166-B*, 979–986.
[16] T. Nomizu, K. Y. Tsukamoto, M. Watanabe, *Anal. Sci.* **2001**, *17*, i177–i180.
[17] K. C. Karli, E. R. Whitby, S. V. Patankar, C. Winstead, T. Ohara, X. Wang, *Appl. Math. Model.* **2001**, 25, 355–373.
[18] G. Gillet, F. Diot, *Miner. Metall. Process.* **1999**, *16*, 1–7.
[19] V. D. Sidorenko, I. A. Gerasimenko, A. M. Kutin, V. B. Yupherov, Ye. I. Skibenko, V. V. Gladky, *IEEE Trans. Magn.* **1996**, *32*, 2691–2694.
[20] L. M. Besley, *Ceram. Dev. Mater. Sci. Forum* **1988**, *34/36*, 941–945.
[21] S. Vieira, A. Aguilo, M. Hortal, M. Pazos, *J. Phys. E: Sci. Instrum.* **1987**, *20*, 1292–1293.
[22] M. Barsoum, D. Patten, S. Tyagi, *Appl. Phys. Lett.* **1987**, *51*, 1954–1956.
[23] K. Hayashi, Y. Yokota, S. Morita, N. Hanada, S. Hayashi, *Jpn. J. Appl. Phys.* **1988**, *27*, 1856–1861.
[24] E. Oba, H. Miyajima, Y. Ishikawa, S. Haseyama, S. Yoshizawa, *Physica C* **1991**, *185/189*, 489–490.
[25] S. Labroo, Y. Ebrahimi, J. Y. Park, W. J. Jeh, *IEEE Trans. Magn.* **1992**, *28*, 1895–1898.
[26] A. C. Pierre, K. Ma, *Eur. J. Solid State Inorg. Chem.* **1993**, *30*, 1083–1094.
[27] S. Labroo, J. Y. Park, R. J. Kearney, W. J. Jeh, *Cryog. Technol.* **1993**, *33*, 1063–1065.
[28] J. H. P. Watson, *J. Appl. Phys.* **1973**, *44*, 4209–4213.
[29] L. Bolt, J. H. P. Watson, *Supercond. Sci. Technol.* **1998**, *11*, 154–161.

[30] M. Marinelli, G. Morpurgo, G. L. Olcese, *Physica C* **1989**, *157*, 149–158.
[31] E. J. Griffith, *Cake Formation in Particulate Systems*, VCH, New York, **1991**.
[32] J. S. Reed in *Principle of Ceramic Processing*, 2nd Ed., Wiley-Interscience, New York, **1995**, pp. 135–1995.
[33] M. A. Abdelgadir, L. Chow, *Hyperfine Interact.* **1999**, *121*, 507–512.
[34] M. A. Abdelgadir, R. S. Burrows, *J. Mater. Res.* **1996**, *11*, 1804–1809.
[35] R. S. Burrows, D. H. McDaniel, M. Abdelgadir, *J. Magn. Magn. Mater.* **1993**, *125*, 269–271.
[36] R. M. Cornell, H. C. U. Schwertmann in *The Iron Oxides*, 2nd Ed., Wiley-VCH, Weinheim, **2003**, pp. 121–123.
[37] N. Saunders, A. P. Miodownik in *CALPHAD—Calculation of Phase Diagrams a Comprehensive Guide*, Elsevier, Oxford, **1998**, p. 1.
[38] P. Kerschl, R. Grössinger, C. Kussbach, R. Sato-Turtelli, K. H. Müller, L. Schultz, *J. Magn. Magn. Mater.* **2002**, *242–245*, 1468–1470.
[39] P. J. Wijin in *Landolt–Börnstein, Vol. 4* (Ed.: K. H. Hellwege), Spinger, New York, **1970**, pp. 572–576 .

Received: March 11, 2004
Published online: August 12, 2004

